

Chapter 1

Trapping of volatile ices during ice mixture desorption

Ice desorption determines the evolution of the gas-phase chemistry during the protostellar stage, and also the composition of comets forming in circumstellar disks. From observations, most CO₂ ice and some CO ice are present in H₂O-dominated ices. This is crucial, since volatile species are easily trapped in H₂O ice and thus desorb with H₂O. Yet, astrochemical models generally treat ice desorption as originating from pure ices. A few studies instead define different ‘flavours’ of CO with different desorption energies, but this approach is limited by lack of information on what fractions of volatile ice are trapped under different conditions. The aim of this study is two-fold: first to experimentally investigate how CO and CO₂ trapping in H₂O ice depends on ice thickness, mixture ratio and heating rate, and second to introduce a modified three-phase (gas, ice surface and mantle) model to treat ice mixture desorption with a minimum number of free parameters. In the experiments the fraction of trapped volatile species increases with ice thickness, H₂O:CO₂/CO mixing ratio and heating rate, resulting 5–17% trapped CO₂ and 2–5% trapped CO with respect to H₂O ice. This is reproduced quantitatively for binary ice mixtures by the modified three-phase model with a single diffusion parameter each for CO, CO₂ and H₂O; these parameters govern the relative diffusion rates between the mantle and the surface for the ice mixture molecules. The model furthermore reproduces the experimental results on dilute tertiary mixtures, but CO₂-rich tertiary ice mixture seems to require a more sophisticated parametrization of diffusion between the surface and mantle layers than currently incorporated. The three-phase model is also used to investigate trapping for astrophysically relevant ice mixtures and time-scales, resulting in ~14% trapped CO₂ ice and 1% trapped CO ice for a 100 ML thick H₂O:CO₂:CO 10:2:1 ice mixture, which significantly less than previously assumed in CO ‘ice-flavour’ models.

⁰Fayolle, E. C., Öberg, K. I., Cuppen, H., Visser, R. and Linnartz, H., in preparation .

1.1 Introduction

Ice-covered interstellar grains constitute a major reservoir of molecules during star formation; in the dense and cold phases of star and planet formation more than 90% of molecules, excluding H_2 , are found in icy grain-mantles (e.g. Bergin et al. 2002). These ices form through direct freeze-out of gas phase atoms and molecules and through their subsequent hydrogenation and oxygenation (Tielens & Hagen 1982, Chapter 2). The most abundant ice molecules are H_2O , CO and CO_2 with typical abundances of $2 \times 10^{-5} - 10^{-4}$ with respect to molecular hydrogen (Gibb et al. 2004; Boogert et al. 2008; Pontoppidan et al. 2008). From their presence in molecular clouds and models, these common ices mainly form in the cold pre-stellar phase (Knez et al. 2005, Chapter 2). Observationally most CO_2 ice is mixed with H_2O ice. Most CO ice is frozen out on top of this H_2O -rich mixture, but a fraction of the CO ice resides in the $\text{H}_2\text{O}:\text{CO}_2$ ice mixture (Tielens et al. 1991; Pontoppidan et al. 2003, 2008, Chapter 2).

Once the pre-stellar core starts to collapse, it heats up the icy grains and the ices start to evaporate. The nature of this desorption process, i.e. which molecules evaporate at which temperatures, dominates the evolution of the gas phase chemistry around the protostar and later in the circumstellar disks (Aikawa et al. 2008; Visser et al. 2009). Understanding ice mixture desorption and implementing the main features of this desorption process in astrochemical networks is therefore crucial when modelling the chemical evolution in protostellar envelopes and in protostellar disks.

Pure ice desorption energies have been determined experimentally for most simple ices, though some values are still contested (e.g. Sandford & Allamandola 1988; Fraser et al. 2001; Collings et al. 2004; Öberg et al. 2005; Brown & Bolina 2007). Laboratory studies on desorption of mixed ices consistently show that the desorption temperatures of mixed ices are different compared to such pure ice desorption (Bar-Nun et al. 1985; Sandford & Allamandola 1988; Collings et al. 2003, 2004). The differences are due to both different binding energies between the mixture components compared to molecules of the same kind, e.g. for $\text{H}_2\text{O}:\text{CO}$ and $\text{CO}:\text{CO}$ the inferred binding energies are ~ 1200 and 830 K, respectively Collings et al. (2003), and because of trapping of volatile species in the hydrogen-bonding ices H_2O and CH_3OH . In most H_2O -rich ice mixtures, volatile mixture components desorb at a minimum of two different temperatures corresponding to desorption from a H_2O surface and from molecules trapped inside the H_2O ice, which only desorb at the onset of H_2O desorption. Additional desorption is sometimes observed at the temperature for pure volatile ice desorption and during ice restructuring, e.g. at the H_2O phase change from amorphous to crystalline. This

H₂O-restructuring is important in ice mixtures dominated by H₂O and occurs at ~140 K in the laboratory (at astrophysical timescales the re-structuring temperature decreases), close to the onset of H₂O-desorption (Collings et al. 2004).

Of the three mixture desorption processes, entrapment of volatile species in H₂O ice is astrochemically most important to quantify. Trapping of CO results in a factor of five increase in the effective desorption temperature. In a recent cloud core collapse model, this would correspond to some CO desorbing 30 AU from the protostar compared to pure CO desorption at 3000 AU. The case is less dramatic, but still significant, for CO₂, which desorbs at ~300 AU when pure and again would desorb at 30 AU if trapped in H₂O ice (Aikawa et al. 2008).

Significant entrapment of volatile species in H₂O ice have been noted in all ice mixture desorption studies above. In addition Sandford & Allamandola (1990) found that CO and CO₂ are trapped in different manners in H₂O ice and that the desorption behaviour depends on whether a dilute mixture is used or a mixture rich in volatile species. Building on this Collings et al. (2004) showed that the fraction of a volatile ice that is trapped in H₂O is generally species specific. From experiments on H₂O:X 20:1 ice mixtures, 16 astrophysically relevant ice species could be divided into three categories dependent on qualitative differences in the desorption behaviour: H₂O-like species (NH₃, CH₃OH and HCOOH) that are completely trapped in the H₂O matrix, CO-like species (N₂, O₂, CO and CH₄) that show some trapping, but all molecules are released during re-structuring, and intermediate species (H₂S, OCS, CO₂, C₂H₂, SO₂, CS₂ and CH₃CN) that display intermediate behaviour.

It is not obvious how this information should be incorporated into astrochemical gas-grain models. There are a few studies, which, using an array of rate equations, can account for all the observed evaporation characteristics of specific, binary ice mixtures (Collings et al. 2003; Bisschop et al. 2006). The molecular specificity of these models, together with a large number of fitting parameters has, however, prevented their incorporation into larger astrochemical models.

Instead, ice desorption is still mostly included into astrochemical models of protostars and disks using the pure ice desorption data, disregarding the possibility of trapping of the volatile molecules in the H₂O matrix (e.g. Aikawa et al. 2008). A few studies on gas-grain interactions during star formation have instead considered a few different flavours of each volatile ice, e.g. the CO ice abundance is split up into one part that evaporates at the pure CO temperature and one part that evaporates at the H₂O evaporation temperature (Viti et al. 2004; Visser et al. 2009). This has provided information on how important ice trapping may be for the chemical evolution during star formation. The approach also allows for the use

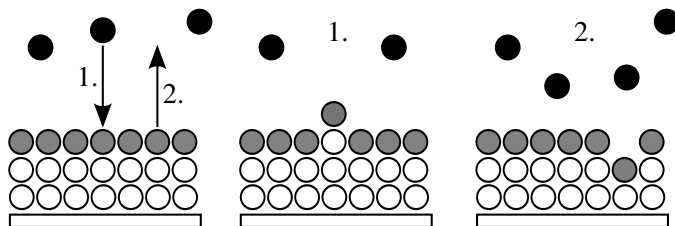


Figure 1.1 A cartoon of desorption and accretion in a three-phase model consisting of mantle molecules (white), surface molecules (grey) and gas molecules (black). Accretion from the gas phase (1.) onto the surface results in the conversion of a surface molecule into a mantle molecule, and similarly desorption (2.) results in the conversion of a mantle molecule into a surface molecule.

of qualitative laboratory results, since different flavour fractions can be assigned to different species based on the classification in Collings et al. (2004). The uncertainties induced by this approach are, however, difficult to ascertain without knowledge of how the amounts of trapped ice depend on different ice variables. The first aim of this study is to provide such information.

Another problem with current gas-grain codes is that evaporation is often incorporated as a first order process, while it is a zeroth order process with respect to the total ice abundance for ices thicker than one monolayer. A three-phase gas-grain model, where the ice mantle and ice surface are treated as two different phases, solves this problem (Fig. 6.1). In a three-phase model desorption is only possible from the surface layer and it is a first order process with respect to surface abundances. The surface is replenished by molecules from the mantle and therefore the desorption kinetics are automatically treated correctly. Such a model also results in ice trapping, since the mantle is protected from desorption. The three-phase model was introduced by Hasegawa & Herbst (1993), but has not been used generally nor has it been further developed, despite its advantages in treating different ice processes. One urgent development is how to couple the surface and the mantle correctly; the original model cannot, for example, account for the experimentally observed different trapping behaviour of different molecules because diffusion rate of all molecules into the surface layer is defined to be species independent.

In this chapter, we suggest that employing a modified form of the three-phase model by Hasegawa & Herbst (1993) allows for a quantitative treatment of evaporation of mixed ices. The model is tested against new data on evaporation from $\text{H}_2\text{O}:\text{CO}$, $\text{H}_2\text{O}:\text{CO}_2$ and $\text{H}_2\text{O}:\text{CO}_2:\text{CO}$ ices, which shows that the three-phase

model can reproduce evaporation quantitatively from binary mixtures and some tertiary ice mixtures in a laboratory setting, while some further improvements are required to reproduce all tertiary results. The laboratory results are also discussed separately with respect to the effects of ice thickness, mixing ratio and heating rate on the amount of trapped ice. This is important information even if another model scheme is preferred to the three-phase model, such as working with different ice flavours. We finally discuss the differences between pure ice evaporation, flavoured ice evaporation and the three-phase model of ice evaporation when the heating-rate is slowed down to 1 K per 100 years, appropriate for low-mass protostars.

1.2 A modified three-phase desorption model

Hasegawa & Herbst (1993) first introduced a three-phase (gas, ice surface and ice mantle) model to address grain-gas interactions and especially ice chemistry. In the context of desorption, the mantle acts as a reservoir of molecules, which replenishes the surface layer during desorption. In the Hasegawa & Herbst (1993) model, this replenishment is statistical, dependent only on the relative concentrations of the different species in the mantle; for a binary mixture A:B, the diffusion rate for a molecule A to reach the surface depends only on the ratio of the mixture in the mantle phase. This results in some desorption for volatile molecules around the pure ice desorption temperature, but also in their trapping, since the surface becomes more and more enriched in the least volatile species as more volatile molecules desorb.

When testing the original three-phase model, it results in too much trapped CO and CO₂ compared to the present experiments. To address this and to include the observed molecular-specific ice trapping into a three-phase model, the ice-mixture dependent rates for mantle molecules to migrate into the surface phase are modified by an experimentally fitted mantle-to-surface diffusion parameter, which is relative to the relative diffusion barriers of the the mixture constituents. Figure 6.2 shows the principal difference between desorption in the traditional three-phase model and a three-phase model, where the diffusion rate of the more volatile species is doubled compared to the less volatile species. This is incorporated into the models through a term P_i for each species i . The equations describing the changes in surface, mantle and gas abundances during desorption for each species i are then

$$\frac{dn_i^s}{dt} = -R_i^{\text{evap}} + \alpha \sum R_i^{\text{evap}} \times \frac{n_i^m}{n^m} P_i, \quad (1.1)$$

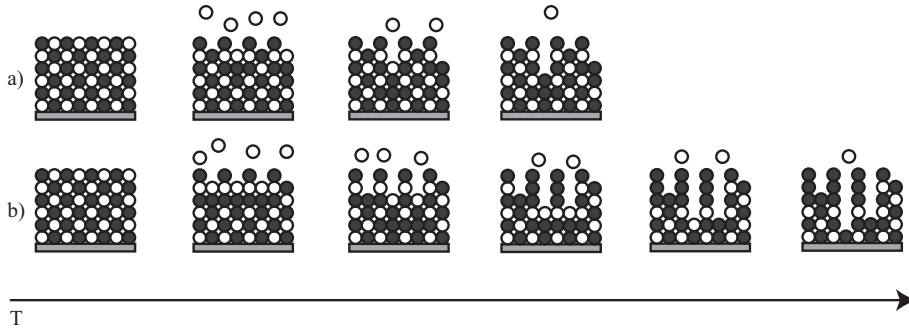


Figure 1.2 A cartoon of desorption within the three-phase model framework from a binary mixture with a volatile component (white) and a non-volatile component (black), which does not desorb at the displayed temperature range. Only surface molecules can desorb. In the traditional model set-up (a) the surface is replenished based on the mantle composition alone, resulting in a large amount of trapped molecules. In our model the mantle-to-surface diffusion is modified such that more volatile species reach the surface faster, reducing the amount of trapped volatile species to fit experimental values.

$$\frac{dn_i^m}{dt} = -\alpha \sum R_i^{\text{evap}} \times \frac{n_i^m}{n^m} P_i, \quad (1.2)$$

$$\frac{dn_i^s}{dt} = R_i^{\text{evap}}, \text{ and} \quad (1.3)$$

$$R_i^{\text{evap}} = n_i^s \times c_i \times e^{-E_i^{\text{evap}}/T} \quad (1.4)$$

where n_i^s , n_i^m , and n_i^g are the abundances of species i in the surface, mantle and gas phase respectively. R_i^{evap} is the evaporation rate for species i which depends on a pre-exponential factor c_i , the evaporation energy barrier E_i^{evap} and the temperature T in Kelvin. α is the ice coverage, which is 1 as long as there is more than one monolayer of ice in the mantle layer, and n^m is the total amount of molecules in the mantle. The modified diffusion rate is modelled as

$$P_i = b_i \times e^{-E_i^{\text{m-s}}/T}, \quad (1.5)$$

where b_i is a normalization factor such that $\sum_i \frac{n_i^m}{n^m} \times P_i = 1$, $E_i^{\text{m-s}}$ is a relative barrier for replacing a desorbed surface molecule with a mantle molecule of species i , which is derived from comparing the model with TPD experiments. The modified

diffusion rate is described with an exponential function, since this kind of expression reproduced the segregation rate as a function of temperature in Chapter 5.

TPD experiments are simulated by solving the rate equations for each time-step (6 seconds) while increasing the temperature linearly with time, using the same heating rates as applied in the laboratory ($0.1\text{--}10\text{ K min}^{-1}$). The other model inputs are the pure ice desorption energies, the diffusion energies, total ice thickness and the ice mixture ratio. The same model can also be used to check the effect of applying an astrophysically relevant heating rate.

The evaporation energies are determined by comparing simulated and laboratory TPD experiments of pure ices and are then set as constants when modelling the mixture desorptions. The $E_i^{\text{m-s}}$ factors are determined empirically by comparing the simulated TPD and experimental TPD outcomes for different binary mixtures. With the model thus constrained, its predictive power is tested by simulating the desorption patterns of other binary and tertiary mixtures using the same values and comparing the simulated and experimental results.

The aim of the model is to predict entrapment of volatile species in the H_2O matrix. In other words, we do aim to perfectly reproduce the experimental desorption curves, e.g. the double-peak around the H_2O ice desorption temperature seen in some experiments. Simulating desorption at such a level of detail does require similar models to what has been used previously to model TPD experiments (Collings et al. 2003).

1.3 TPD experiments

All evaporation experiments are carried out under ultra-high vacuum conditions ($P \sim 10^{-9}$ mbar) in the set-up CRYOPAD, which is described in detail by Fuchs et al. (2006) and Öberg et al. (2005). Pure gas samples and gas mixtures are prepared separately. The ices are grown *in situ* by exposing a cold substrate at the center of the vacuum chamber to a steady flow of gas, directed along the surface normal. Evaporation is induced by linear heating of the substrate (and ice) in Temperature Programmed Desorption (TPD) experiments. The evaporated gas phase molecules are detected by a Quadropole Mass Spectrometer (QMS). The desorption onset in the TPD curves can be directly related to the desorption energy in a pure ice (e.g. Fraser et al. 2001).

The set-up is also equipped with a Fourier transform infrared (FTIR) spectrometer in reflection-absorption mode (reflection-absorption infrared spectroscopy or RAIRS). The FTIR covers $750 - 4000\text{ cm}^{-1}$, which includes at least one vibrational band for each of the investigated molecules, and is run with a spectral

resolution of 1 cm^{-1} . RAIR spectroscopy, together with previously determined band strengths for this RAIRS set-up (Öberg et al. 2009a,b), is used to determine the ice mixture composition in each experiment and to estimate the absolute ice thickness.

Table 6.1 lists the experiments in this study. The ice constituents, abundance ratios, thickness and heating rate are varied to investigate the dependencies of ice mixture desorption on different experimental variables. Isotopologues with ^{13}C were used in some of the experiments to ensure that small contaminations in the chamber do not influence the results. The CO and CO_2 gas both have a minimum 99% purity (indugas). The H_2O sample was prepared from deionized H_2O followed by several freeze-thaw cycles.

The trapped fractions of CO_2 and CO are listed both with respect to the initial CO_2 and CO abundances and the H_2O ice abundance, since both measures are used in the literature. The fractions of trapped ice were calculated by integrating the TPD curves; the fraction of trapped CO_2/CO with respect to the initial CO_2/CO ice content is defined as the ratio of the integrated desorption curve above 100 K and the integrated desorption curve between 20 and 160 K. The trapped fraction is calculated by multiplying this number with the initial CO_2/CO abundance with respect to the initial H_2O ice. RAIR spectra were also acquired during the desorption in some of the experiments, but a lack of accurate band strengths for trapped CO and CO_2 limits their quantitative use.

The ice thicknesses in Table 6.1 have absolute uncertainties of $\sim 50\%$ and relative uncertainties of $\sim 20\%$. The heating rate is accurate within a few percent and the amount of trapped ice within $\sim 20\%$ of the reported percentage values.

1.4 Results

The results are presented in three parts, starting with the experimental results on binary ice mixtures, followed by the model results on binary ice mixtures and experiments and models of tertiary ice mixtures.

1.4.1 Experimental TPD curves of binary ice mixtures

Figure 6.3 shows the desorption curves of CO_2 and CO from H_2O dominated ice mixtures together with pure CO and CO_2 TPD curves. As reported in previous studies on H_2O -rich mixtures, the volatile species desorb both around the desorption temperature of the pure ice and around the H_2O desorption temperature. CO and CO_2 mixture desorption differ, however, in the onset of the first mixture

Table 1.1 The TPD experiments.

Composition	Ratio	Thick. (ML)	Heating rate (K min ⁻¹)	Trapped CO/CO ₂ ice	
				% CO ₂ /CO ice	% H ₂ O ice
H ₂ O	-	24	1		
¹³ CO ₂	-	6	1		
¹³ CO	-	6	1		
H ₂ O:CO ₂	10:1	11	1	65	7
H ₂ O:CO ₂	10:1	18	1	77	8
H ₂ O:CO ₂	10:1	36	1	85	9
H ₂ O: ¹³ CO ₂	4:1	~11	10	46	12
H ₂ O: ¹³ CO ₂	4:1	~11	1	40	10
H ₂ O: ¹³ CO ₂	4:1	~11	0.1	37	9
H ₂ O: ¹³ CO ₂	4:1	~28	10	68	17
H ₂ O: ¹³ CO ₂	4:1	~28	1	64	16
H ₂ O: ¹³ CO ₂	4:1	~28	0.1	60	15
H ₂ O: ¹³ CO	5:1	19	1	24	5
H ₂ O: ¹³ CO	2:1	16	1	<13	<7
H ₂ O: ¹³ CO	2:1	6	1	<12	<6
H ₂ O:CO ₂ :CO	~11:4:1	16	1	32/17	12/2
H ₂ O:CO ₂ :CO	~20:1:1	30	1	92/96	5/5

desorption peak compared to the onset of pure ice desorption; the CO₂ peak is slightly shifted towards lower temperatures compared to the pure ice, while the CO desorption from the H₂O mixture is shifted to a ~5 K higher temperature. This can be understood if CO₂ forms weaker bonds in a H₂O ice compared to a CO₂ ice, while CO forms stronger bonds with H₂O than to itself, confirming the assumptions made when simulating ice segregation in Chapter 5.

Similarly to Fig. 6.3, the TPD curves of all investigated ice mixtures contain two desorption peaks, though the fractions of trapped CO₂/CO in the H₂O ice vary significantly between the different experiments, dependent on ice composition, ice mixing ratio, ice thickness and heating rate during the TPD experiments.

These dependencies are displayed in Figure 6.4, which shows the experimental CO and CO₂ TPD curves from most of the binary ice mixture experiments listed in Table 6.1 together with the pure ice desorption curves (bottom curves). The heating rate is 1 K min⁻¹, except for where noted otherwise. Comparing the

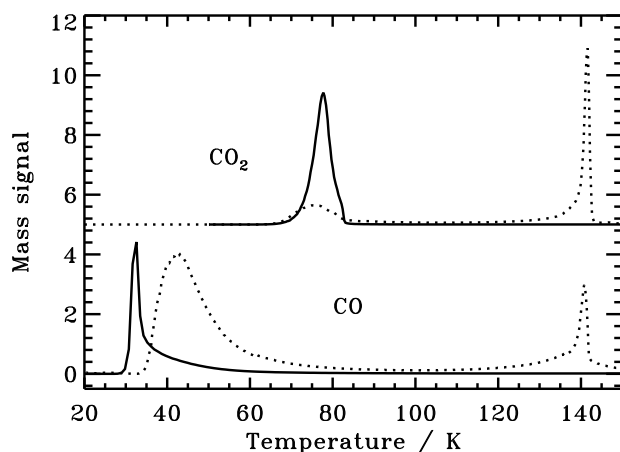


Figure 1.3 Desorption of CO and CO₂ from pure ices (solid lines) and H₂O:CO 5:1 and H₂O:CO₂ 4:1 ice mixtures (dotted lines). The TPD curves have been normalized with arbitrary factors for visibility.

TPD curves of CO₂ desorption from the 11 ML thick H₂O:CO₂ 4:1 ice mixture and of CO desorption from the 19 ML thick H₂O:CO 5:1 ice mixture, shows that CO₂ is easier trapped of the two, in agreement with previous studies.

Starting at the top of the figure, a larger fraction of CO ice with respect to the initial CO abundance is retained in the H₂O ice in the more dilute ice mixtures. This is true for CO₂ as well. The next set of curves show that increasing the heating rate increases the amount of trapped CO₂ and shifts the desorption curves to higher temperatures – the standard heating rate is 1 K min⁻¹. Quantitatively the fraction of trapped CO₂ increases from 60 to 68% of the total CO₂ abundances or 15–17% of the H₂O abundance when the heating rate is raised from 0.1 to 10 K min⁻¹. This is barely significant, but the trend seems to be real. The middle curves demonstrate the previously noted dependence on mixture ratio by plotting the TPD curves for CO₂ desorption from H₂O:CO₂ 10:1 and 4:1, 11 ML thick ice mixtures. The amount of trapped volatiles also depends on the ice thickness. The next to last set of curves shows how the amount of trapped CO₂ increases for the H₂O:CO₂ 10:1 ice mixtures between 11 and 36 ML (Fig. 6.4).

As mentioned above, the trapped ice fractions for all experiments are reported in Table 6.1, where the amount of trapped volatile ice is defined both with respect to the initial volatile ice content and the initial H₂O abundance. The trapped fractions of CO₂ vary between 37 and 85% with respect to the initial CO₂ ice and

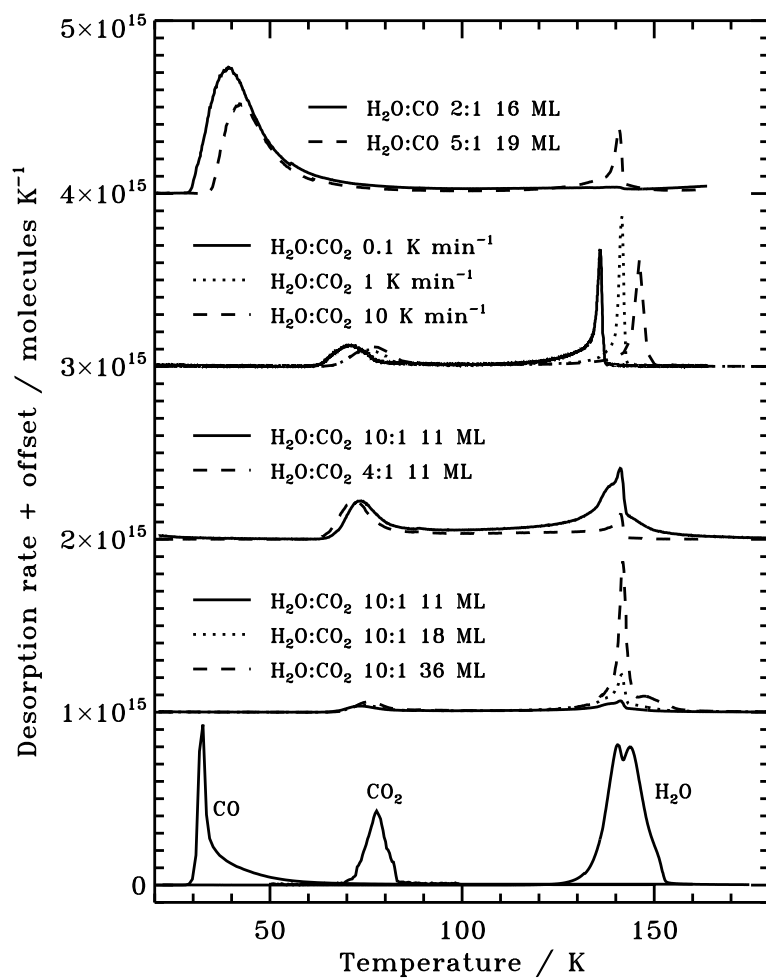


Figure 1.4 Experimental CO and CO₂ TPD curves during warm-up of ice mixtures (offset for visibility), together with pure CO, CO₂ and H₂O ice TPD curves (bottom curves). The heating rate is 1 K min⁻¹. The TPD curves are scaled to correspond to the spectroscopically measured ice abundances when integrating the desorption curves.

between 5 and 17% with respect to H₂O. The trapped CO amounts between <12% and 24% with respect to CO, and 2% and 5% with respect to H₂O.

Simulations of binary ice mixtures

Figure 6.5 shows the simulated CO and CO₂ TPD curves for the ice mixtures investigated experimentally in Fig. 6.4. The desorption energies are derived from the experimental and simulated pure ice TPD curves (bottom curves) to be $E_{\text{H}_2\text{O}}^{\text{des}} = 4850$ K, $E_{\text{CO}_2}^{\text{des}} = 2475$ K and $E_{\text{CO}}^{\text{des}} = 1050$ K, assuming a pre-exponential factor of 10^{12} s⁻¹, which are in reasonable agreement with typical literature values within the ~20% uncertainties, though a higher binding energy has been reported for H₂O (Fraser et al. 2001). To keep the model simple, these binding energies are used to model ice mixture desorption as well, since the differences in binding energies for CO and CO₂ in H₂O ice mixtures do not affect the amount of trapped ice in the model.

Regardless of the choice of relative diffusion rates, the three-phase model reproduces the experimental trends with respect to mixture ratio, heating rate and ice thickness, shown here for a specific set of diffusion parameters (Fig. 6.5). This is intuitive when referring back to Fig. 6.2, which shows first that all ice is trapped below a certain ice depth and thus the trapped fraction will increase with ice thickness. Second, reducing the concentration of the volatile component will result in a faster cover of the surface by H₂O and third, when the heating rate is increased, the H₂O desorption temperature will be reached before all volatile species that could potentially reach the surface layer do so.

The shapes of the simulated curves deviate from the experimental curves for a couple of reasons. First, the model does not take into account that the pumping rate of desorbed species is limited in the experiment, which partly explains the tail during CO desorption. The model does also no account for multiple desorption sites with different binding energies or the desorption due to H₂O re-structuring around 140 K.

Similarly to the experiments, the simulated ice trapping during binary mixture desorption are quantified through the fractions of the volatile ice species that desorb below and above 100 K. The trapped CO and CO₂ fractions in the experiments and models agree quantitatively for a chosen set of binary ices when the relative ‘diffusion barriers’ are set to be $E_{\text{H}_2\text{O}}^{\text{m-s}} = 970$ K, $E_{\text{CO}_2}^{\text{m-s}} = 665$ K and $E_{\text{CO}}^{\text{m-s}} = 617$ K. These $E^{\text{m-s}}$ values are derived from a subset of experiments and then used to model all TPD curves in Fig. 6.5. The CO₂ diffusion barrier is derived from comparing experiments and simulations of the three 10:1 ice experiments and the

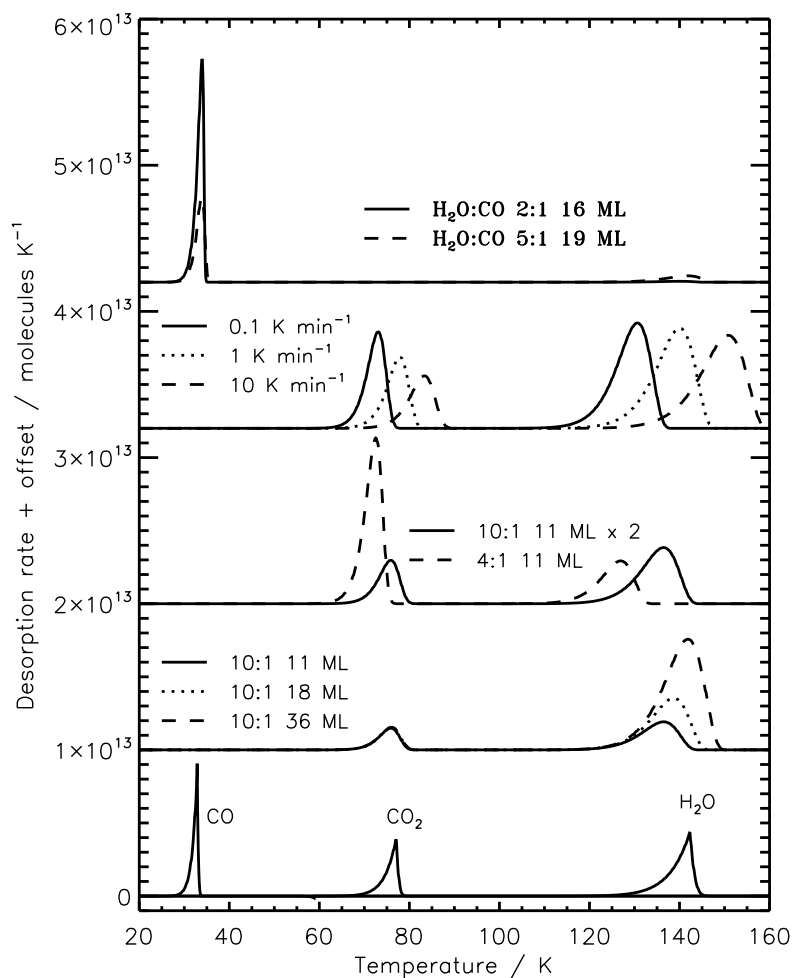


Figure 1.5 Simulated CO and CO₂ TPD curves from pure ices, from H₂O:CO₂ 10:1 ice mixture of different thicknesses, from 11 ML H₂O:CO₂ 10:1 and 4:1 ice mixtures, from 28 ML H₂O:CO₂ 4:1 mixtures heated at different rates and from H₂O:CO ice mixtures.

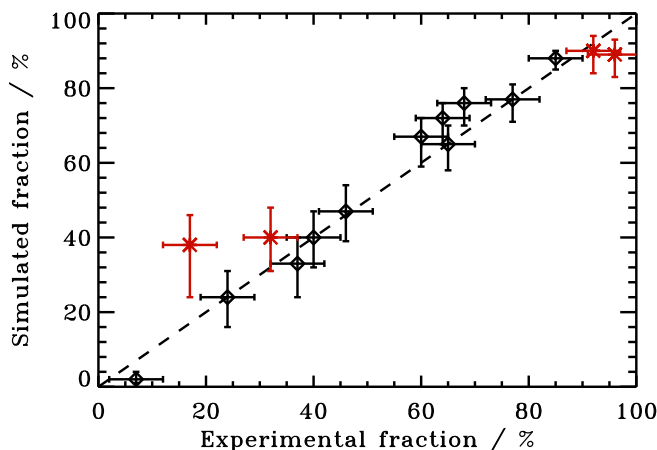


Figure 1.6 The experimental and simulated CO and CO₂ ice fractions trapped in the H₂O ice during ice mixture desorption for all the investigated ice compositions, mixture ratios, thicknesses and heating rates. The dashed line indicates the position of a one-to-one correlation. The crosses indicate tertiary ice experiments.

CO value is derived from the 5:1 experiment, while the H₂O value was arbitrarily chosen ahead of the fitting procedure; other sets of diffusion parameters may reproduce the experiments as well, since it is only the relative diffusion rates of H₂O and CO or CO₂ that determines the desorption behaviour in the binary ices.

Figure 6.6 shows the fraction of the volatile ice trapped in the H₂O ice for experiments versus simulations using the derived relative diffusion barriers. The uncertainties include the measurement of the ice fractions and the choice of ice thickness and mixing ratio in the simulations when aiming to mimic the experiments. Within the uncertainties the simulations reproduce all binary ice mixture results quantitatively.

1.4.2 Tertiary ice mixtures

Figure 6.7 shows the experimental and simulated TPD curves of two tertiary H₂O:CO₂:CO ice mixtures with different mixture compositions, one CO₂-rich mixture and one dilute mixture. The simulations are run with the parameters from the binary mixtures without any further attempt to optimize the fit.

Qualitatively the 20:1:1 mixture seems well reproduced by the simulation (top sets of TPD curves), while the simulation of the 11:4:1 mixture releases too little

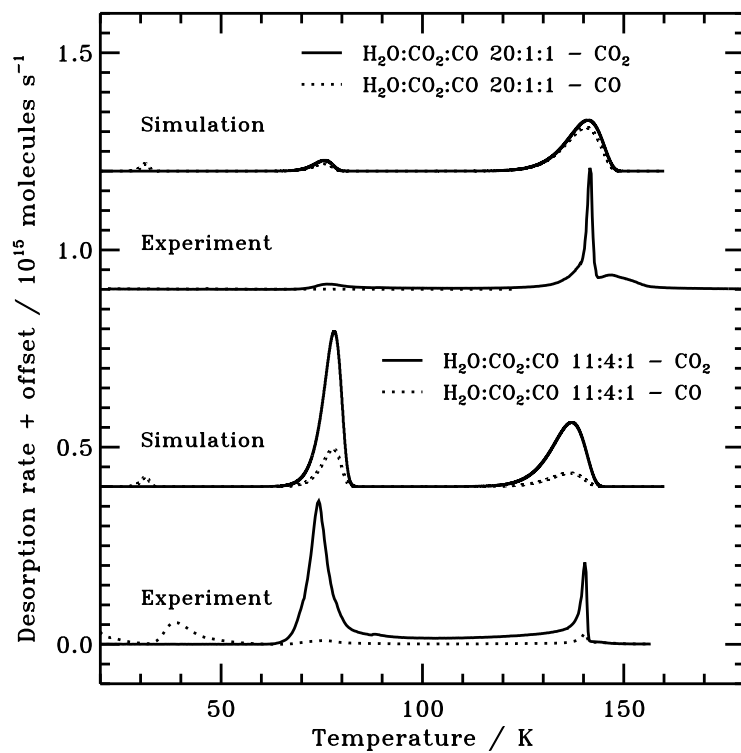


Figure 1.7 Simulated and experimental CO and CO₂ TPD curves from tertiary H₂O:CO₂:CO ice mixtures. The heating rate is 1 K min⁻¹ and the ice thicknesses 16 ML for the 11:4:1 ice mixture and 30 ML for the 20:1:1 ice mixture.

CO at the pure CO temperature and too much together with CO₂ (bottom sets of TPD curves). The fraction of CO trapped in H₂O is also predicted too be large in the CO₂-rich experiment, 38% with respect to the initial CO content compared to the experimentally observed 17%.

The experimental and simulated amounts of CO and CO₂ trapped in the H₂O ice are overplotted in Fig. 6.6. Quantitatively the model predicts the correct amounts of trapped CO and CO₂ in the dilute mixture and of trapped CO₂ ice in the CO₂-rich tertiary mixture.

1.5 Discussion

1.5.1 Desorption from ice mixtures

Qualitatively the experimental results agree with those published by Collings et al. (2004) in the sense that CO₂ is more efficiently trapped than CO. Viti et al. (2004) quantified the trapped amounts of CO and CO₂ in the experiments by Collings et al. (2004) to model ice desorption around a protostar. They find that 30% CO and 90% CO₂ is trapped in H₂O ice, which are both high compared to most of the present experiments. The differences can be understood from the very dilute mixtures used by Collings et al. (2004), 20:1, when investigating ice desorption.

This difference between the previous and present experimental results together with the experimental TPD curves show that the fraction of trapped ice (whether measured with respect to volatile ice content or H₂O ice abundance) varies dependent on ice thickness, mixing ratio and heating-rate, which will vary in astrophysical environments as well. In other words, there is no constant fraction of CO or CO₂ ice that is trapped in a H₂O-dominated ice. In addition, the decreasing amount of CO₂ trapped in the H₂O ice as the heating rate is slowed down suggests that the trapping of volatile species is due to very slow diffusion of volatile species within a H₂O matrix rather than an actual entrapment that molecules cannot escape from. The opposite conclusion could be drawn by Sandford & Allamandola (1988) based on high-vacuum experiments with thick ices. This confirms the different dynamics of thin and thick ices found for ice segregation in Chapter 5.

The desorption results are furthermore consistent with the simulations of ice segregation in Chapter 5, where swapping of bulk molecules was invoked to explain the observed slow bulk diffusion. Slow bulk diffusion also explains that more volatile ice is trapped in the thicker ices where the average diffusion path to the surface layer is longer. The decrease in the amount of trapped volatile ice with higher concentrations of volatiles is also consistent with the ice segregation ex-

periments, where the segregation rate increases with concentration of the volatile species.

In the tertiary mixtures, CO₂ desorption is not significantly affected by the presence of CO and the amount of trapped CO₂ is consistent with a H₂O:CO₂ mixture with the same mixture ratio and ice thickness. CO is affected by the presence of large amounts of CO₂. Less CO is trapped in the mixture with ~36% CO₂ with respect to H₂O ice than in an equivalent binary H₂O:CO mixture, indicative of a lower diffusion barrier for CO in the CO₂-rich H₂O-mixtures compared to diffusion in H₂O:CO ices. This may be the result of CO₂ disrupting the hydrogen-bonding network (Sandford & Allamandola 1990, Chapter 4).

1.5.2 The three-phase desorption model

The modified three-phase model was set up to quantify the amounts of CO and CO₂ ices that desorb at the H₂O desorption temperature during ice mixture desorption with a minimum number of equations and fitting parameters.

The modified three-phase model reproduces the fraction of trapped ices in the experimental binary TPD curves for all different ice thicknesses, mixing ratios, heating rates and compositions with only one free parameter per species in addition to the pure desorption energies. To parametrize binary ice desorption from H₂:CO and H₂O:CO₂ ices thus only requires fitting one of the experiments to the model, though an averaged value from fits with three experiments was used for the H₂O:CO₂ ice mixtures. The other experimental results were then accurately predicted, within the experimental uncertainties, with the same parameters, except for CO desorbing from a CO₂-rich tertiary H₂O-ice mixture. Overall the simple parametrization of diffusion between the mantle and the surface used in this version of the three-phase model is thus sufficient.

The fact that the current model reproduces desorption from binary ice mixtures suggests that diffusion between the top ice layer and the layer right beneath it is efficient, while bulk diffusion is slow – consistent with the analysis of the experiments above. In other words, if a H₂O molecule reaches the surface because a CO₂/CO molecule desorbs from right on top of it, there is a high probability that it will swap places with an underlying CO₂/CO molecule. This process is what the modified three-phase model approximates by increasing the diffusion rate of volatile molecules to the surface and decreasing it for H₂O, compared to the original diffusion rates based on the mantle composition alone (Hasegawa & Herbst 1993). The decrease in water diffusion must equal the increase in diffusion of CO₂/CO, since the model in its current state does not allow for back-diffusion between the surface and the mantle.

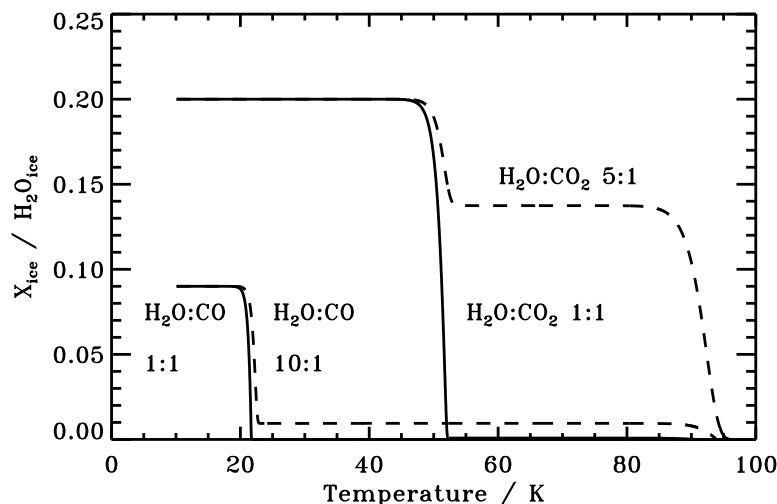


Figure 1.8 The amount of CO and CO₂ ice during ice warm-up with 1 K per 100 years according to the three-phase model, assuming two different initial ice mixtures with H₂O.

Monte Carlo simulation including diffusion and desorption similar to those performed in Chapter 5 should however be used to demonstrate that this simple scheme of fast surface swapping and slow bulk swapping during warm-up of ices is sufficient to explain the experimental results and the successes of the modified three-phase model in reproducing them.

1.5.3 Astrophysical implications

Trapping of volatile ices in H₂O ice is a crucial parameter when predicting the chemical evolution during star and planet-formation. Understanding the uncertainties in model predictions of ice trapping is therefore important in e.g. ice-flavour models, but has so far not been evaluated. The modified three-phase desorption model is used here to test the effects of different initial ice compositions and ice thicknesses on ice mixture desorption. This can either be used to design ice flavour models. Ultimately the three-phase model should, however, be integrated with a protostellar collapse model to model ice desorption realistically during star formation.

Figure 6.8 shows the amount of CO and CO₂ ice with respect to the original H₂O ice abundance as a function of temperature, assuming two different initial

binary ice compositions, a total H₂O ice thickness of 100 ML and a heating rate of 1 K per 100 years. The different initial conditions are based on ice observations towards protostars (Chapter 2). The CO₂ observations show that H₂O:CO₂ generally co-exist and have an abundance ratio of 5 to 1. In contrast most CO ice is in a pure layer on top of the H₂O-ice mixture, but some CO mixed in with the H₂O ice at a 1 to 10 ratio.

The initial ice H₂O:CO₂ composition is first set to H₂O:CO₂ 5:1, which assumes that all H₂O and CO₂ are initially mixed together. A H₂O:CO₂ 1:1 36 ML thick ice is also investigated, since from infrared spectroscopy of protostellar ices, we do not know whether all H₂O and CO₂ are mixed together or whether H₂O forms partly as a pure ice and then a H₂O:CO₂ mixture forms on top, corresponding to an ice composition of H₂O:CO₂ 1:1/4 (Chapter 4). Similarly, the initial H₂O:CO ice conditions are set to H₂O:CO 10:1 100 ML and H₂O:CO 1:1 18 ML. In all four cases the CO₂ and CO ice fractions are reported with respect to the total amount of H₂O ice, i.e. 100 ML. Thus the initial CO₂ and CO fractions are always 20 and 10% with respect to H₂O, respectively.

Starting with these compositions, Fig. 6.8 shows that almost no volatile ice is trapped in the 1:1 ice mixtures – the results of these compositions are not significantly different from assuming pure ice desorption. The H₂O:CO₂ 5:1 ice models result in that most of the CO₂ ice is trapped; at the onset of H₂O desorption the ice mixture contains ~14% of CO₂ ice with respect to the initial H₂O ice abundance. A smaller amount of CO is trapped in the 10:1 ice, ~1% with respect to the H₂O ice abundance. This is an order of magnitude lower than the values used in Visser et al. (2009) and Viti et al. (2004) and shows the importance of modelling experimental results rather than assuming that a specific experiment can be used to generally predict processes under astrophysical conditions.

Based on these results, it will be difficult to explain more than a few percent of CO in comets, from CO trapped in H₂O ice during the pre- or proto-stellar stages.

1.5.4 Future development – towards a four-phase model

While this version of the three-phase model already provides some advantages in treating ice mixture desorption compared to previous attempts, it does have two areas that need further development. The first one is quite obviously a more accurate treatment of desorption of CO and other very volatile species from CO₂-rich H₂O-ice mixtures, whether tertiary ices or more complex. This may be solved by having relative diffusion probabilities that are constantly redefined in the model based on the ice composition according to some simple formula.

A second approach is to allow for continuous diffusion between the surface

and mantle layer. This would require a revision of the current set of rate equations, since the three-phase model is set up such that the mantle to surface diffusion rate is identical to the ice desorption/accretion rate. It should however be possible to implement. In addition this more general approach is advantageous when using the three-phase model in the future to investigate ice chemistry.

A second challenge is how to deal with the astrophysical reality of two different ice mantle phases, a H₂O-rich ice phase and a CO-rich ice phase (Chapter 2). It is worth considering whether a four-phase model is necessary to produce realistic ice models both with respect to desorption and ice chemistry. At low temperatures the complex ice chemistry may for example be very different if CH₃OH fragments can only react with CO and other CH₃OH fragments and not with NH₃ and CH₄ fragments. Such a four-phase model would however be more complicated than most kinds of three-phase models and will only be attempted after diffusion between the mantle and the surface in the three-phase model has been successfully modelled.

1.5.5 Conclusions

Desorption from H₂O-rich ice mixtures is complex in that the amount of trapped ice depends not only on the species involved, but also on the mixture ratio, the ice thickness and the heating rate – there is no constant fraction of volatile species trapped in a H₂O ice. This ‘complex’ behaviour can, however, be reproduced by a small improvement of the three-phase model by Hasegawa & Herbst (1993). Using pure ice desorption energies and one diffusion parameter for H₂O, CO₂ and CO each, the modified three-phase model can reproduce the amount of trapped ice quantitatively in all binary ice mixtures investigated, even though the diffusion parameter was fitted using only a few H₂O:CO₂ experiments and a single H₂O:CO experiment. The same three diffusion parameters also predict trapping accurately in H₂O-dominated tertiary H₂O:CO₂:CO ice mixtures, while desorption from a CO₂-rich tertiary mixture requires a more sophisticated parametrisation of diffusion in the ice than is currently implemented.

Extrapolating the model results to astrophysical heating rates and a plausible H₂O:CO₂:CO 10:2:1 ice composition results in ~14% CO₂ and ~1% CO, with respect to H₂O ice, trapped inside of the H₂O ice. Trapping of CO in H₂O ice may thus be an order of magnitude less efficient than previously assumed. In previous models, experimental results on a H₂O:CO 20:1 mixture were assumed to translate directly to astrophysical conditions with a more CO-rich ice; the experiments and models here show that this is not a reasonable simplification. This further strengthens the underlying theme in this thesis that experimental studies

must explore the entire parameter space available before extrapolating the results to astrophysical settings.

References

- Aikawa, Y., Wakelam, V., Garrod, R. T., & Herbst, E. 2008, *ApJ*, 674, 984
- Bar-Nun, A., Herman, G., Laufer, D., & Rappaport, M. L. 1985, *Icarus*, 63, 317
- Bergin, E. A., Alves, J., Huard, T., & Lada, C. J. 2002, *ApJL*, 570, L101
- Bisschop, S. E., Fraser, H. J., Öberg, K. I., van Dishoeck, E. F., & Schlemmer, S. 2006, *A&A*, 449, 1297
- Boogert, A. C. A., Pontoppidan, K. M., Knez, C., et al. 2008, *ApJ*, 678, 985
- Brown, W. A. & Bolina, A. S. 2007, *MNRAS*, 374, 1006
- Collings, M. P., Anderson, M. A., Chen, R., et al. 2004, *MNRAS*, 354, 1133
- Collings, M. P., Dever, J. W., Fraser, H. J., & McCoustra, M. R. S. 2003, *Ap&SS*, 285, 633
- Fraser, H. J., Collings, M. P., McCoustra, M. R. S., & Williams, D. A. 2001, *MNRAS*, 327, 1165
- Fuchs, G. W., Acharyya, K., Bisschop, S. E., et al. 2006, *Faraday Discussions*, 133, 331
- Gibb, E. L., Whittet, D. C. B., Boogert, A. C. A., & Tielens, A. G. G. M. 2004, *ApJS*, 151, 35
- Hasegawa, T. I. & Herbst, E. 1993, *MNRAS*, 263, 589
- Knez, C., Boogert, A. C. A., Pontoppidan, K. M., et al. 2005, *ApJ*, 635, L145
- Öberg, K. I., Linnartz, H., Visser, R., & van Dishoeck, E. F. 2009a, *ApJ*, 693, 1209
- Öberg, K. I., van Broekhuizen, F., Fraser, H. J., et al. 2005, *ApJL*, 621, L33
- Öberg, K. I., van Dishoeck, E. F., & Linnartz, H. 2009b, *A&A*, 496, 281
- Pontoppidan, K. M., Boogert, A. C. A., Fraser, H. J., et al. 2008, *ApJ*, 678, 1005
- Pontoppidan, K. M., Fraser, H. J., Dartois, E., et al. 2003, *A&A*, 408, 981
- Sandford, S. A. & Allamandola, L. J. 1988, *Icarus*, 76, 201
- Sandford, S. A. & Allamandola, L. J. 1990, *ApJ*, 355, 357
- Tielens, A. G. G. M. & Hagen, W. 1982, *A&A*, 114, 245
- Tielens, A. G. G. M., Tokunaga, A. T., Geballe, T. R., & Baas, F. 1991, *ApJ*, 381, 181
- Visser, R., van Dishoeck, E. F., Doty, S. D., & Dullemond, C. P. 2009, *A&A*, 495, 881
- Viti, S., Collings, M. P., Dever, J. W., McCoustra, M. R. S., & Williams, D. A. 2004, *MNRAS*, 354, 1141